J. Fluid Mech. (2007), *vol.* 573, *pp.* 89–104.
doi:10.1017/S0022112006003880 Printed in the United Kingdom

A jet-like structure revealed by a numerical simulation of rotating spherical-shell magnetoconvection

ATARU SAKURABA

Department of Earth and Planetary Science, University of Tokyo, Tokyo, Japan

(Received 18 March 2005 and in revised form 7 August 2006)

Numerical results on thermally driven nonlinear magnetoconvection in a rapidly rotating fluid spherical shell are reported. A uniform magnetic field that is parallel to the rotation axis is imposed externally. The Ekman number is 2×10^{-6}, representing a state of negligible viscosity, as in the Earth's core. The convection pattern is characterized by a few large-scale vortex columns superimposed on a fast westward (retrograde) zonal flow. In the equatorial region, an anticyclonic vortex is intensified, in which an induced axial magnetic field is stored. Interaction between the magnetized vortex and the zonal flow leads to a thin jet at the western side of the vortex. The jet is also characterized by a thin electric current sheet caused by a steep gradient of the axial magnetic field. Because of this structure, the jet region can be designated as a magnetic front by analogy with fronts in mid-latitude atmospheric cyclones. It can be estimated from an order-of-magnitude analysis that the jet width decreases in inverse proportion to the zonal flow speed, and that the jet speed and the sheet-like electric current are proportional to the square of the zonal flow speed.

1. Introduction

Convection in the Earth's liquid core has distinctive features originating from its spherical geometry, self-gravitation, rapid rotation and high electrical conductivity, which are all indispensable ingredients of the process of magnetic field generation (a geodynamo). To elucidate such geodynamic phenomena, including convection in planetary cores, self-excited magnetohydrodynamic dynamos in rotating spheres have been studied using three-dimensional numerical simulations (e.g. Glatzmaier & Roberts 1995; Kuang & Bloxham 1997). Convection in the presence of an applied magnetic field (magnetoconvection) in rotating spherical geometry has also been investigated using linear (Fearn 1979; Zhang 1995; Walker & Barenghi 1997; Sakuraba 2002) and nonlinear calculations (Olson & Glatzmaier 1995; Sarson *et al.* 1997; Walker & Barenghi 1999; Sakuraba & Kono 2000), which provides a more fundamental understanding. This paper follows the latter path.

It was recognized in these studies that the Ekman number

$$E = \frac{\nu}{2\Omega R_0^2}, \tag{1.1}$$

representing the ratio of viscous to Coriolis forces in the equation of motion, is an important non-dimensional parameter, where Ω is the angular velocity of the core, R_0 its radius and ν its kinematic viscosity. A realistic value of E in the Earth is $O(10^{-9})$, even with a turbulent viscosity. In most direct numerical simulations of Earth-type

dynamos or magnetoconvection, however, the Ekman numbers are not smaller than 10^{-5}. Some authors have implemented models with smaller values but assuming hyperviscosity to artificially damp small-scale flows, or some kind of symmetry in numerical solutions (see reviews by Zhang & Schubert 2000; Kono & Roberts 2002). Without the restrictions of spherical geometry or a magnetic field, convection at Ekman numbers less than 10^{-5} has been realized by recent numerical (Stellmach & Hansen 2004) and experimental studies (Aubert *et al.* 2001; Sumita & Olson 2003).

How small an Ekman number is sufficient to represent a convective state of the Earth's core? The answer is complex. In a rapidly rotating system, an increase in a magnetic field makes the viscous force unimportant, except in various thin shear layers, because the Lorentz force due to an induced electric current can play the role of the viscous force. In such a strong-field state, therefore, the convection pattern is invariant with a change of E by definition. In a rapidly rotating system there are disparities between its strong-field and weak-field limits (Zhang & Schubert 2000). A remarkable feature might be that the ratio of magnetic to kinetic energy densities increases in proportion to E^{-1} in the strong-field limit, but it is constant in the weak-field limit. In the former case, a flow is constrained by Lorentz and Coriolis forces, but it remains unclear what kind of flow pattern occurs. In most previous direct numerical simulations, this energy ratio does not exceed 100 and is typically around $O(10)$, whereas it reaches several thousand or greater in the Earth's core. It has been inferred from studies of simplified magnetoconvection in spherical geometries (Dormy, Cardin & Jault 1998; Sakuraba 2002) that an Ekman number of $O(10^{-5})$ is insufficiently small. It should be at least $O(10^{-6})$ to achieve a convective regime of negligible viscosity such that the disparities become clearer.

In this study a nonlinear calculation of rotating spherical magnetoconvection is carried out for a parameter space of $E = O(10^{-6})$, smaller by one order of magnitude than the previous studies, which we hope is a first step towards extracting some fundamental features inherent to low-E magnetoconvection. As in Sarson *et al.* (1997) and Sakuraba & Kono (2000), a uniform magnetic field parallel to the rotation axis is applied externally so that a magnetohydrodynamic interaction ensues at a moderate Reynolds number. The uniform field is not merely simple, it is also force-free and represents a crude approximation of the Earth's poloidal (dipole) field. In other studies, a toroidal (azimuthal) field has been preferred as the basic field. However, toroidal and poloidal fields are coupled inside the core so that a seed magnetic field can be either toroidal or poloidal provided its pattern and amplitude are appropriate. A toroidal basic field causes magnetic instability under some conditions (Fearn 1979), making it difficult to investigate the thermally driven magnetoconvection that this paper is intended to examine.

An important parameter of rotating magnetoconvection is the Elsasser number

$$\Lambda = \frac{\sigma B_0^2}{2\rho\Omega}, \tag{1.2}$$

where B_0 is the characteristic intensity of the basic field, σ is the electrical conductivity and ρ is the fluid density. According to linear studies (e.g. Fearn 1979), the critical Rayleigh number at the onset of thermally driven magnetoconvection decreases with increasing Λ; it reaches an overall minimum when $\Lambda = O(1)$. This behaviour is also shown in the present configuration, where the basic field is uniform and parallel to the rotation axis and the axes of convection rolls are also almost parallel to them (Sakuraba 2002). Nonlinear studies (Cardin & Olson 1995; Olson & Glatzmaier 1995; Sakuraba & Kono 2000) show that the convection type changes dramatically between

the cases of $\Lambda < 1$ (a weak-field state) and $\Lambda > 1$ (a strong-field state). In the Earth's core, the Elsasser number is inferred to be of order unity if B_0 is the self-excited magnetic field intensity. These facts indicate that a convective system naturally reaches a state in which the Elsasser number of the induced magnetic field becomes $O(1)$ and the Lorentz and Coriolis forces are basically balanced. To elucidate such a strong-field state, we specifically examine the case of $\Lambda = 1$ in this paper.

2. Model

The model consists of a spherical shell (outer core) that is filled with an electrically conductive Boussinesq fluid and of an insulating medium outside it, comprising a mantle and inner core. The core is spun with a constant angular velocity $\Omega \boldsymbol{e}_z$ and is permeated by a uniform magnetic field $B_0 \boldsymbol{e}_z$, where $\boldsymbol{e}_z$ is the unit vector along the z-axis and co-rotation of the mantle and the inner core is assumed. We simulate three-dimensional time-dependent thermal convection by solving the following equations:

$$E_m \frac{\partial \boldsymbol{u}}{\partial t} = E\nabla^2 \boldsymbol{u} + E_m \boldsymbol{u} \times \boldsymbol{\omega} - \nabla\left(p + \tfrac{1}{2} E_m \boldsymbol{u} \cdot \boldsymbol{u}\right) + \boldsymbol{u} \times \boldsymbol{e}_z + \boldsymbol{J} \times \boldsymbol{B} + q Ra T \boldsymbol{r}, \tag{2.1}$$

$$\frac{\partial \boldsymbol{B}}{\partial t} = \nabla^2 \boldsymbol{B} + \nabla \times (\boldsymbol{u} \times \boldsymbol{B}), \tag{2.2}$$

$$\frac{\partial T}{\partial t} = q\nabla^2 T - \boldsymbol{u} \cdot \nabla(\overline{T} + T), \tag{2.3}$$

and $\nabla \cdot \boldsymbol{u} = \nabla \cdot \boldsymbol{B} = 0$. They are in a reference frame rotating with the core, where $\boldsymbol{u}$, $\boldsymbol{B}$, $\boldsymbol{\omega} = \nabla \times \boldsymbol{u}$, $\boldsymbol{J} = \nabla \times \boldsymbol{B}$, p and T are, respectively, the velocity, magnetic field, vorticity, electric current density, and pressure and temperature perturbations from a hydrostatic state in which the temperature is $\overline{T} = 1/r$ and the fluid rotates rigidly. The equations are non-dimensionalized with characteristic scales of length R_0, time R_0^2/η, velocity η/R_0, magnetic field $(2\rho\Omega\mu_0\eta)^{1/2}$, temperature βR_0 and pressure $2\rho\Omega\eta$, where $\eta = 1/(\mu_0\sigma)$ is the magnetic diffusivity, μ_0 is the magnetic permeability and β is the gradient of temperature at the core–mantle boundary (CMB) in the hydrostatic state. The non-dimensional velocity and magnetic field respectively represent the magnetic Reynolds and Elsasser numbers with this scaling. The (modified) Rayleigh number $Ra = \alpha\beta g_0 R_0^2/(2\Omega\kappa)$, the magnetic Ekman number $E_m = \eta/(2\Omega R_0^2)$ and the diffusivity ratio $q = \kappa/\eta$ are derived as non-dimensional parameters in addition to E, where α is the thermal expansivity and κ is the thermal diffusivity. The acceleration due to gravity is g_0 at the CMB and is assumed to be proportional to the distance from the core's centre.

The velocity satisfies rigid boundary conditions. The magnetic field is continuous everywhere and connects to potential fields outside the core. The potential field far from the core approaches the uniform axial field $\Lambda^{1/2}\boldsymbol{e}_z$, where Λ is the Elsasser number of the applied field. The temperature at the inner core boundary is fixed to an initial value, whereas the heat flux is laterally homogeneous at the CMB. The mean temperature at the CMB is fixed to maintain a constant temperature difference across the fluid shell. Therefore, the heat flux across the CMB increases because of convective heat transport. The velocity and the magnetic field are decomposed into poloidal and toroidal fields. Equations governing the defining scalars of the poloidal and toroidal fields in addition to (2.3) are reduced to a system of ordinary differential equations using a spectral method based on spherical harmonic and Chebyshev expansions, with the pressure term eliminated by taking the curl of (2.1). Time-stepping is employed using a predictor–corrector method with diffusion terms treated

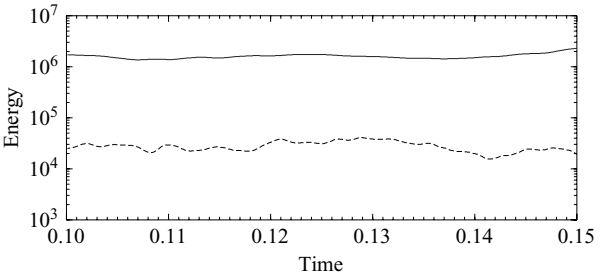

FIGURE 1. The induced magnetic energy (solid line) and kinetic energy (broken line) stored in the fluid shell plotted as functions of time.

by an implicit Crank–Nicolson method. We specifically examine a parameter set $E = E_m = 2 \times 10^{-6}$, $Ra = 200$, $q = 1$ and $\Lambda = 1$ in this paper, with a non-dimensional inner core radius of 0.35. Although the magnetic Prandtl numbers $P_m = E/E_m$ and q are both small in the Earth's core, they are set to unity so that a magnetic field can be induced by moderate convective motion. The maximum degree and order of the spherical harmonics are both 159 and the maximum degree of the Chebyshev polynomials is 96.

A linear stability calculation (Sakuraba 2002) predicts that the critical Rayleigh number for this parameter set is 150. The even modes of $m = 0$ and 1 and the odd modes of $0 \leqslant m \leqslant 2$ both give approximately this critical Rayleigh number, where m is the azimuthal wavenumber and the even (odd) mode is characterized by radial velocity symmetric (antisymmetric) with respect to the equatorial plane ($z = 0$) and by a magnetic field with axial dipole (quadrapole) symmetry. The linear calculation also predicts that, in the absence of the magnetic field, the most unstable mode is an even mode of $m = 24$ and the critical Rayleigh number is 330, indicating that the system would be stable without the magnetic field. This is the reason why magnetoconvection is studied in this paper despite the same computational complexity as in self-exciting dynamos. We can avoid high Rayleigh numbers and observe magnetohydrodynamic interactions in well-controlled conditions.

3. Results and interpretation

3.1. *Overview of convective structure*

Calculation is begun from the initial condition that the temperature perturbation is random and of small amplitude. Only even-mode perturbations grow selectively; the resultant solution has even-mode (dipole) symmetry. At a quasi-steady state, the induced magnetic energy density, $\frac{1}{2}E_m^{-1}|\boldsymbol{B} - \Lambda^{1/2}\boldsymbol{e}_z|^2$, is, on average, more than 50 times greater than the kinetic energy density, $\frac{1}{2}|\boldsymbol{u}|^2$ (figure 1). This implies that a magneto-geostrophic balance among Coriolis, Lorentz, pressure and buoyancy forces is well-established.

Figure 2(a) shows a snapshot of fluid motion in the equatorial plane at the time when an unusual flow structure emerges ($t = 0.12$). The velocity field around the inner core is dominated by a westward (retrograde) zonal flow prevailing up to around the mid-depth of the fluid shell. The outer part of the shell has nearly stationary vortices. The zonal flow has a wave-like structure with large scales that resemble westerlies in the atmosphere. The most striking feature is that a strong inward-flowing jet forms on the downstream side of a bulge of the wave-like zonal flow. One noteworthy jet is

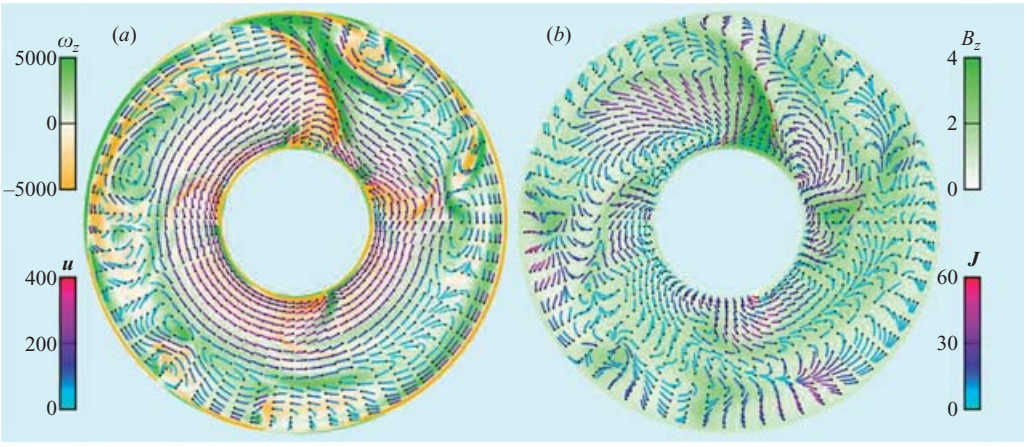

FIGURE 2. (*a*) A convection pattern on the equatorial plane viewed from the north ($z > 0$). The axial vorticity ω_z is represented as a colour map and the velocity $\boldsymbol{u}$ by instantaneous streamlines starting from dots. The colour of the streamline indicates the flow speed, whereas its length is arbitrary. (*b*) The electromagnetic field pattern corresponding to (*a*). The axial magnetic field B_z is shown by a colour map and the electric current $\boldsymbol{J}$ is shown by streamlines.

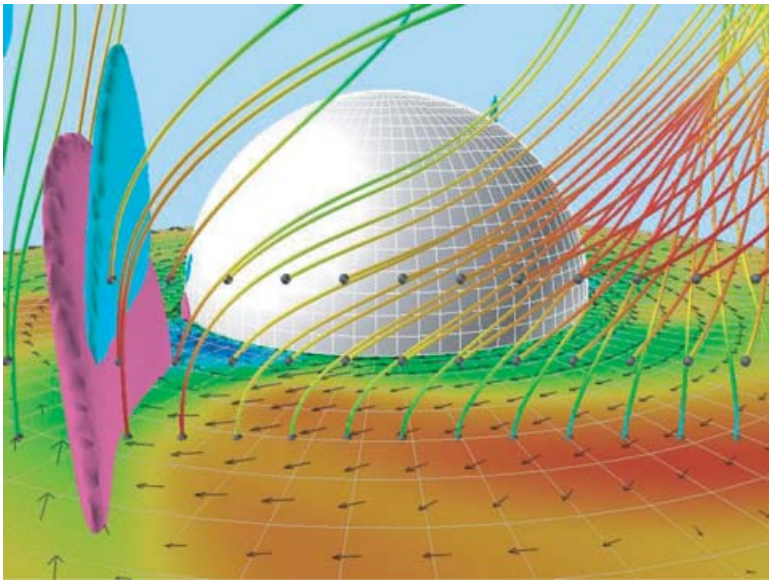

FIGURE 3. An oblique view of the northern half of the fluid shell at the same time as figure 2. Shoehorn-like pink and light blue objects respectively depict the isosurfaces of $(u_s^2 + u_\phi^2)^{1/2} = 400$ and $u_z = 200$, where (s, ϕ, z) are the cylindrical coordinates. The colour of the equatorial plane shows the temperature perturbation (red for $T \geqslant 1$ and blue for $T \leqslant -1$) and arrows represent the velocity field. The jet shown in figure 2(*a*) corresponds to the equatorial section of the pink isosurface. Magnetic field lines are drawn from dots and their intensity is designated by colours (red for $|\boldsymbol{B}| \geqslant 4$ and blue for $|\boldsymbol{B}| = 0$). The dots are spaced equally on a vertical plane that is 0.6 from the z-axis. The inner core is shown as a grey hemisphere.

illustrated in figure 2(*a*) by red streamlines on a pair of adjacent narrow vorticity bands. The maximum Reynolds number is greater than 750 at the centre of the jet. Figure 2(*b*) depicts the electromagnetic field at the same time as figure 2(*a*). It is apparent that the axial magnetic field is intensified considerably at the east of the jet. At the same place as the inward flowing jet, there is a strong jet-like electric current, which is shown as red lines with opposite direction to that of the fluid jet. The peak electric current density is greater than 100 at that moment.

The jet structure extends in the z-direction to around $|z| < 0.3$, as shown in figure 3. The horizontal component (u_s, u_ϕ) is dominant in the jet region, but vertical flows (u_z) are not negligible at some distance from the equatorial plane, where (u_s, u_ϕ, u_z) are the velocity components in the cylindrical coordinates (s, ϕ, z). It is noteworthy that a gap exists between the centres of the horizontal and vertical jets, which will be discussed later. The jet drifts westward and its strength exhibits an intermittent behaviour, as shown in figure 4. In this paper, a flow structure is designated as a jet only when the velocity is higher than 500 and the electric current density, which is antiparallel to the velocity vector, is greater than 80. With these criteria, jet-like structures are found at $t = 0.120$, 0.129 and 0.145 in figure 4. The jet lifetime is typically 0.003 in non-dimensional units and its retrograde angular velocity is about $2\pi/0.02 = 310$ rad per unit time. In the following subsections, a possible mechanism of the formation of this unusual jet is described in detail.

3.2. *Zonal flow*

The westward zonal flow circulating around the inner-core equator can be interpreted as a thermal wind. A hot plume rises from the inner-core equator and warms the equatorial part of the fluid shell. Four plumes are visible in figure 2, but their shape is severely changed by the zonal flow. When averaged in the azimuthal direction, the equatorial plume is followed by poleward flows beneath the CMB and equatorward counterflows along the cylindrical surface tangent to the inner-core equator (figure 5). These meridional circulations inevitably create a zonal flow in the equatorial part of the shell so that the inward Coriolis force balances the outward buoyancy force.

On the equatorial plane, the axial and azimuthal components of the vorticity equation (the curl of (2.1)) are reduced to

$$E_m\left(\frac{\partial \omega_z}{\partial t} + \boldsymbol{u}\cdot\nabla_h \omega_z\right) + \boldsymbol{J}\cdot\nabla_h B_z = (1+E_m\omega_z)\frac{\partial u_z}{\partial z} + B_z\frac{\partial J_z}{\partial z} - qRa\frac{\partial T}{\partial \phi}, \tag{3.1}$$

$$0 = (1+E_m\omega_z)\frac{\partial u_\phi}{\partial z} + B_z\frac{\partial J_\phi}{\partial z} + qRa\frac{\partial T}{\partial z}, \tag{3.2}$$

and those of the induction equation (2.2) are

$$\frac{\partial B_z}{\partial t} + \boldsymbol{u}\cdot\nabla_h B_z = B_z\frac{\partial u_z}{\partial z} + \nabla^2 B_z, \tag{3.3}$$

$$0 = B_z\frac{\partial u_\phi}{\partial z} + \nabla^2 B_\phi, \tag{3.4}$$

where $\nabla_h = \boldsymbol{e}_s(\partial/\partial s + s^{-1}) + \boldsymbol{e}_\phi s^{-1}\partial/\partial\phi$. Here, we have assumed that the solution belongs to an even mode and that the viscous force is negligible. These equations are also approximately valid in the vicinity of the equatorial plane. A well-known thermal wind relationship is derived from (3.2) if the nonlinear and the Lorentz force terms are neglected. In general, the relationship can be written as

$$\frac{\partial u_\phi}{\partial z} - qRa\frac{\partial T}{\partial \theta} = 0, \tag{3.5}$$

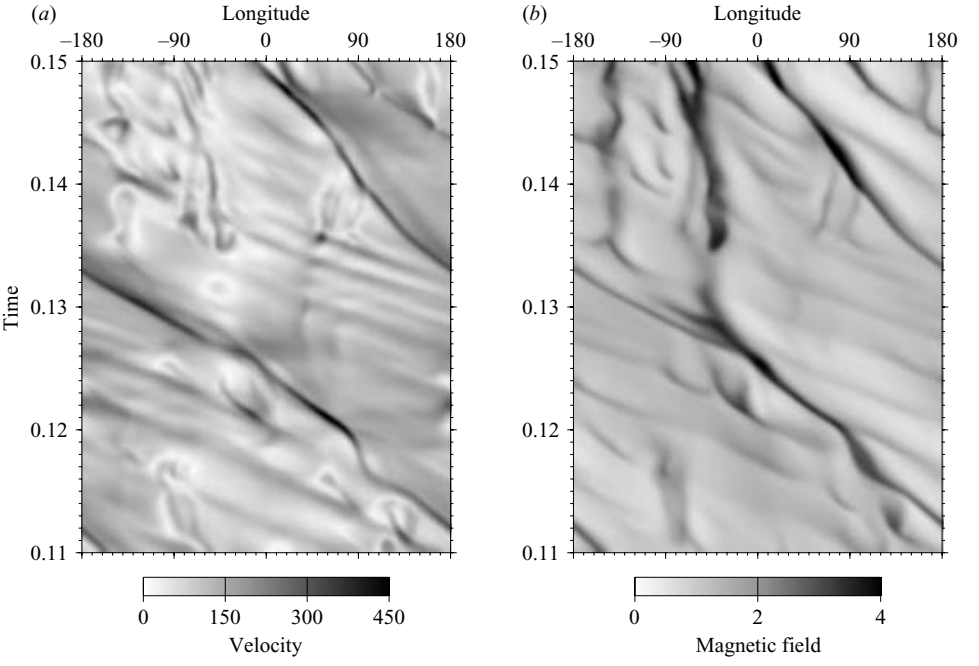

FIGURE 4. (*a*) The horizontal flow amplitude ($(u_s^2+u_\phi^2)^{1/2}$) and (*b*) the vertical magnetic field (B_z) on $z=0$ and $s=0.675$ are shown by grey shades as functions of longitude and time. A jet is visualized by a black band in (*a*). It is apparent that the jet is located at the western edge of a magnetic field maximum and moves westward.

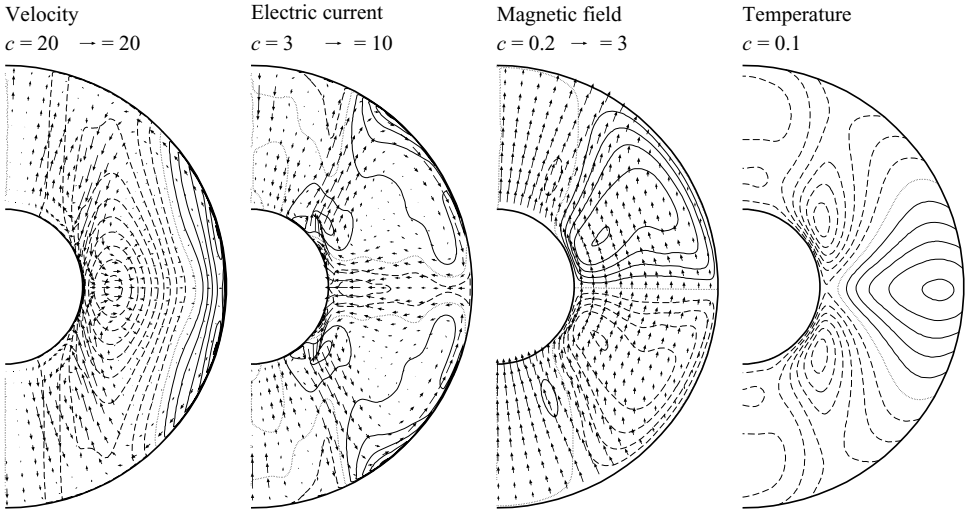

FIGURE 5. The velocity, electric current, magnetic field and temperature averaged both in time and longitude. The temperature and the zonal components of the vector variables are plotted by contour maps on the meridional plane with solid lines representing positive values. The arrows represent meridional components. In each panel, the contour interval c and the value corresponding to a unit arrow length are shown.

where θ denotes the colatitude in the spherical coordinates. Figure 5 depicts $\partial T/\partial\theta \simeq 0.8/(\pi/4) \simeq 1$ and $\partial u_\phi/\partial z \simeq 120/0.5 = 240$ in the central part of the meridional section, which agrees with the fact that $qRa = 200$ in this simulation. Zonal flows are similarly found in other calculations of Earth-type dynamos and magnetoconvection (e.g. Olson & Glatzmaier 1995; Kuang & Bloxham 1997). The mechanism has also been recognized to be a thermal wind and the magnetic effect of less importance in the azimuthally averaged equation of motion (Aubert 2005).

Variation of the mean zonal flow in the presence of an axial magnetic field creates a toroidal magnetic field, as predicted by (3.4). That generation mechanism is known as an ω-effect and is readily apparent in figure 5. Figure 3 also illustrates how magnetic field lines are advected and distorted as a result of the shear of the zonal flow. The azimuthally averaged meridional flows and electric currents are almost antiparallel as shown in figure 5, reflecting the balance between the zonal components of the Coriolis and Lorentz forces in a magneto-geostrophic state. In fact, those vectors are exactly antiparallel if the magnetic field is axial and uniform. Note that the direction of the electric current depends on the applied field; it would be parallel to the velocity field if the applied field were $-\Lambda^{1/2}\boldsymbol{e}_z$.

3.3. *Magnetic field generation and hollow vortex*

The first term in the right-hand side of (3.3) is a stretching term to intensify the axial field near the equatorial plane. Assuming a geostrophic balance, one can relate this term to $\partial T/\partial\phi$ from (3.1). A hot plume upwelling from the inner-core equator produces a temperature difference $\partial T/\partial\phi > 0$ in its west side, where an anticyclonic vortex ($\omega_z < 0$) exists. Consequently, the axial magnetic field is intensified at the anticyclonic vortex near the equatorial plane (Kageyama *et al.* 1995). This tendency is also apparent in results obtained in this paper (see figures 2 and 3).

The negative vorticity is noticeably concentrated in a thin narrow area, whereas the magnetic field maximum (located in the eastern side of the jet) is rather broad. We consider this discrepancy to be related to a hollow vorticity structure in an anticyclone, as reported by Ishihara & Kida (2002). The mechanism of formation of the hollow anticyclone has not yet been explained quantitatively, but it can be roughly interpreted as follows. The concentrated axial magnetic fluxes push the surrounding fluid outward because of the Lorentz force that is diametrically opposite to the Coriolis force in the anticyclone. It is well known that the presence of a magnetic field considerably reduces the critical Rayleigh number for the onset of rotating thermal convection and enlarges the cell size (Chandrasekhar 1961). This effect is also relevant in the present case, in which a uniform axial basic field is applied to a rotating fluid sphere (Sakuraba 2002). A conventional explanation for it is that the Coriolis force, which typically suppresses convection, is partly cancelled by a Lorentz force. In a rotating spherical convection with an even-mode symmetry, a balance is established in the equatorial part of the anticyclonic vortex. In consequence, the anticyclonic fluid circulations dominate over a large area and play the most important role in heat transport (Sakuraba & Kono 1999, 2000). Because a conducting fluid cannot easily flow across lines of magnetic force, the fluid circulates around the rim of the large magnetized anticyclone and a stagnant hollow emerges at the centre. The magnetic field inside broadens as a result of magnetic diffusion.

3.4. *Formation of the jet and current sheet*

The jet-like structure would not be apparent if the angular velocity of the westward zonal flow were constant and it had no shear in the s-direction. The situation considered here is that the zonal wind is westward near the inner-core equator, whereas

it is eastward in the outermost part of the core (figure 5). Therefore, temperature and magnetic fields, and also a vorticity field that is linked to them, are advected in a complicated manner. Figure 4 illustrates an almost stationary trend and fast westward drifting of velocity and magnetic field patterns, reflecting the coexistence of the stagnant part near the CMB and the fast thermal wind circulating around the inner-core equator.

The magnetic flux lines around the equatorial plane are confined in an enlarged anticyclone, as described in previous subsections, and are advected westward with it. In the course of this process, the magnetized anticyclone collides with an almost stationary unmagnetized (cyclonic) vortex that exists in the outer part of the fluid shell. The magnetic field is 'dammed' at the collision boundary because of weak magnetic diffusion compared to the effect of advection. Then, the intensity of the axial magnetic field changes drastically across the boundary and an electric current sheet forms there. The concomitant Lorentz force is balanced partly by an inertial force but mainly by a Coriolis force, which is provided by the formation of a strong jet parallel to the current sheet.

The process of jet formation described above is apparent in figure 4. At $t = 0.12$, for example, two B_z maxima merge and then a jet-like flow ensues. Detailed examination of this process reveals that the leading B_z maximum slows (the collision process) and is caught by with the following weak B_z maximum (the damming effect). The electric current sheet and the fluid jet simultaneously form and move westward with nearly the same speed as the thermal wind when the magnetic field becomes sufficiently strong. This feature is commonly seen in other cases.

Figure 6 illustrates a local structure of the jet on the equatorial plane. The axial magnetic field increases suddenly in the jet region; subsequently, it becomes gradually decreasing function of longitude in the upstream side. Because of this field pattern, the jet can be designated as a magnetic front by analogy with a front in a mid-latitude cyclone, where hot and cold air masses collide and a steep temperature gradient occurs. The electric current vector (black arrows) flips at the front and a sharp increase of its magnitude is observed. The velocity field tends to be *antiparallel* to the electric current so that the Lorentz force is balanced by the Coriolis force.

The axial components of the velocity and the electric current also have a tendency to be opposite, as is indicated by figure 6(*b*). The jet away from the equatorial plane (vertical jet) originates from an already existing axial flow inside the anticyclone, which stretches and concentrates the axial magnetic field there (see § 3.3). At the time when the electric current sheet and the jet form because of the collision of the vortices, the axial flow is pushed against the magnetic front. In this process, the magnetic force plays an important role. As described in § 3.2, there exists a prograde zonal magnetic field in the northern hemisphere because of the ω-effect. The thin jet stretches the zonal field to create locally antiparallel radial magnetic fields. That is, in the northern hemisphere, the jet pulls the magnetic field $B_\phi > 0$ so that an inward radial magnetic field $B_s < 0$ is induced in the western side of the jet and an outward field $B_s > 0$ is induced in the eastern side. Consequently, a sheet-like vertical (equatorward) electric current forms at almost the same place as the magnetic front. This can also be understood as an electric current induced by the $\boldsymbol{u} \times \boldsymbol{B}$ field, where $\boldsymbol{u}$ is the jet velocity and $\boldsymbol{B}$ is the zonal field. The balance between the Lorentz and the Coriolis forces near the equatorial plane yields the coexistence of u_z and J_z (see (3.1)). Therefore, the axial flow is forced to be localized at the magnetic front, and the vertical jet ensues. It should be noted that the vertical flow away from the equatorial plane induces B_z (see (3.3)) and sustains the jet structure itself. That is, the horizontal

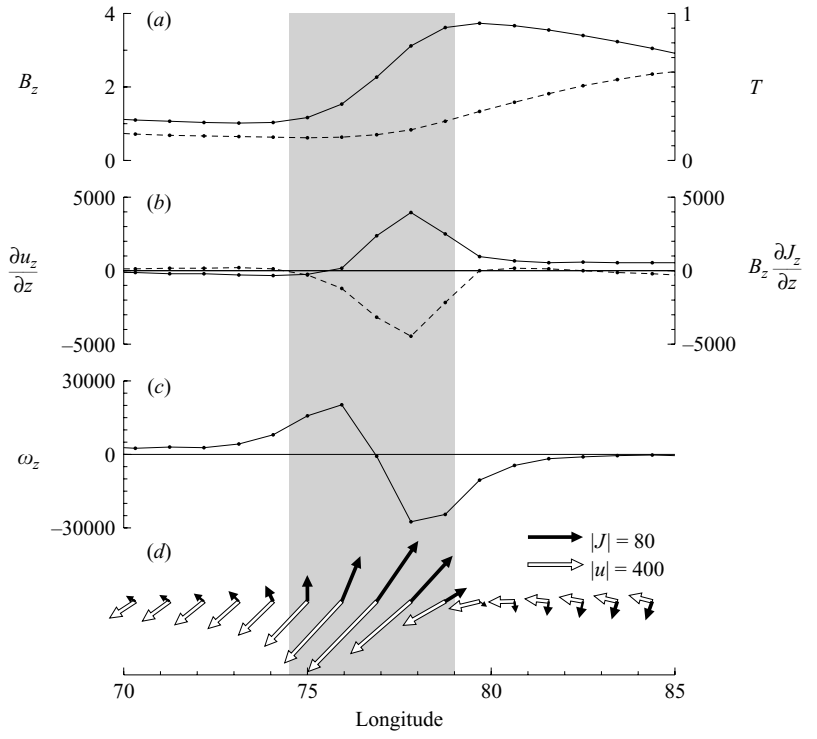

FIGURE 6. (*a*) The axial magnetic field (B_z; solid line) and the temperature perturbation (T; broken line) on $z=0$ and $s=0.675$ and at $t=0.12$ are shown as functions of longitude. (*b*) Similarly, $\partial u_z/\partial z$ (solid line), $B_z\partial J_z/\partial z$ (broken line) and (*c*) ω_z are shown. (*d*) Velocity and electric currents parallel to the equatorial plane on the same traversing line are represented respectively by white and black arrows. The horizontal and vertical projections of each arrow respectively represent its ϕ and s components. The grey part roughly represents the jet region.

and vertical jets and the electric current sheet in the presence of the axial and zonal magnetic fields comprise a self-sustaining system that maintains the frontal structure. For this reason, the jet continues for some time (figure 4).

Figure 6(*a*) shows that the temperature does not exhibit a sudden change at the magnetic front, indicating that the jet is not of thermal origin, but rather of electromagnetic origin. This fact can be verified by the variation pattern of the axial vorticity. Figure 6(*c*) indicates that ω_z is generated not by a thermal torque, but by a magnetic one (see (3.1)).

The hollow anticyclonic vortex has a noteworthy intrinsic characteristic: it is accompanied by a circulating flow that is localized on its outer rim. The circulating flow on the downstream side is amplified because of the relative growth of the magnetic field if the magnetic field stored in the flow is advected in the presence of a fast zonal wind. On the other hand, it is weakened on the upstream side because the magnetic field is advected away. The jet formation can be also interpreted as an asymmetric growth of the magnetized hollow anticyclone caused by its nonlinear interaction with a fast zonal wind.

In this calculation, the viscous force is unimportant, even in the thin jet; its magnitude is less than 3% of the Lorentz force magnitude. It is generally found that the Lorentz force has half the magnitude of the Coriolis force at the magnetic front. The remaining part is balanced mainly by pressure and buoyancy forces and partly

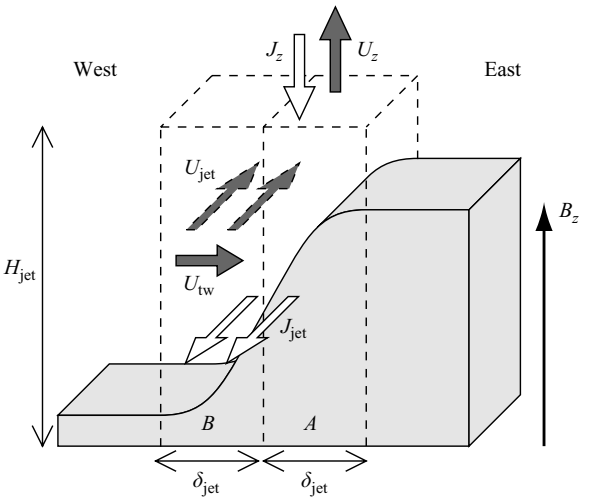

FIGURE 7. Illustration of a magnetic front viewed from a reference frame moving with it. Grey and white arrows respectively represent directions of flows and electric currents. The intensity of an axial field B_z is expressed by the height of the solid object. The jet region (divided into A and B) is shown by rectangular boxes bordered with broken lines. The thermal wind $U_{\rm tw}$ is prograde (eastward) here because of the coordinate transformation.

by an inertial force, which is at most 10% of the Lorentz force. When velocity and magnetic fields change with amplitudes U and B respectively, and with a common length scale L, the ratio of the inertial force to the Lorentz force can be written as

$$\frac{|E_m(\boldsymbol{u}\cdot\nabla)\boldsymbol{u}|}{|\boldsymbol{J}\times\boldsymbol{B}|} \simeq \frac{E_m U^2/L}{B^2/L} = \frac{\frac{1}{2}U^2}{\frac{1}{2}E_m^{-1}B^2}, \tag{3.6}$$

which is equal the ratio of non-dimensional kinetic to magnetic energy densities. This quantity is much smaller than unity if averaged in the whole core (see figure 1). Even in the narrow jet, it is only 0.1 if we take $U = 700$ and $B = 3$ as typical values. When a magnetized anticyclone collides with an unmagnetized vortex and a steep gradient of the magnetic field emerges, the Lorentz force perpendicular to the collision boundary produces a jet along the boundary because there are no strong inertial and viscous forces. Only the Coriolis force acts to oppose the Lorentz force. We can conclude that the reduction of inertial and viscous forces in a system of low E is one cause of the jet formation.

3.5. *Estimate of the frontal structure*

The magnetic front moves westward at an equal or lower speed than the thermal wind velocity $U_{\rm tw}$. As shown in figure 2, the thermal wind blows onto the front and makes a right-angled turn there to form a narrow jet toward the inner core. Because the magnetic front does not extend in the radial direction, its phase velocity differs slightly from $U_{\rm tw}$. In any case, it appears as if there is an invisible wall along the magnetic front at which the thermal wind changes its direction. When viewed from a reference frame moving with the magnetic front, the jet structure is nearly time-independent, as portrayed in figure 7. For the sake of simplicity, let us assume that the magnetic front is exactly radial (parallel to $\boldsymbol{e}_s$) and that its phase velocity coincides with $U_{\rm tw}$. The jet is conceptually separable into two parts. In the eastern side (region A), the magnetic field stretching due to of the vertical jet U_z compensates diffusion due to the sharply

varying magnetic field B_z. Note that the location of the vertical jet differs slightly from the maximum of the horizontal component $U_{\rm jet}$, as shown in figures 3 and 6. In the western side (region B), on the other hand, the magnetic diffusion balances advection of the axial field. Assuming a sinusoidal variation of B_z in the magnetic front, one obtains from (3.3) that

$$B_z \frac{U_z}{H_{\rm jet}} \simeq \frac{\pi^2 B_z}{2\delta_{\rm jet}^2}, \quad U_{\rm tw} \frac{\pi B_z}{2\delta_{\rm jet}} \simeq \frac{\pi^2 B_z}{2\delta_{\rm jet}^2} \tag{3.7}$$

in regions A and B, respectively, or

$$\delta_{\rm jet}^{-1} \simeq \frac{1}{\pi}\sqrt{\frac{2U_z}{H_{\rm jet}}} \simeq \frac{U_{\rm tw}}{\pi}, \tag{3.8}$$

where $\delta_{\rm jet}$ is the half-width of the jet region and $H_{\rm jet}$ is the height. Substituting $U_{\rm tw} = 180$ and $\partial u_z/\partial z \simeq U_z/H_{\rm jet} = 4000$ gives $\delta_{\rm jet} = 1/30$–$1/60$ (see figure 6). This value is comparable with the observational value $\delta_{\rm jet} = 1/40$, the difference being caused by horizontal advection of a magnetic field along the jet. Note that $H_{\rm jet}$ in this estimation is about 0.05 because u_z grows sharply near the equatorial plane. Therefore, there would be a difference from the height of the jet in the usual sense (see figure 3). Taking account of mass conservation

$$U_{\rm tw} H_{\rm jet} D_{\rm jet} \simeq U_z \delta_{\rm jet} D_{\rm jet} + U_{\rm jet} \delta_{\rm jet} H_{\rm jet}, \tag{3.9}$$

one can obtain proportionality relations

$$\delta_{\rm jet} \propto U_{\rm tw}^{-1}, \quad U_{\rm jet} \propto D_{\rm jet} U_{\rm tw}^2, \quad U_z \propto H_{\rm jet} U_{\rm tw}^2, \tag{3.10}$$

where $D_{\rm jet}$ is the depth of the jet region. Because these estimates are derived without considering equations of motion and heat transport, the values of $U_{\rm tw}$ and B_z cannot be obtained. Nevertheless, relations (3.10) are useful for estimating the jet structure based on a zonal flow speed.

One might imagine a jet in the Earth's core if the structure of the magnetic front were universal in low-E magnetoconvection. The flow in the Earth's core has been estimated through theoretical, experimental and observational studies (e.g. Aurnou *et al.* 2003; Hulot *et al.* 2002). Nevertheless, it is still difficult to evaluate its speed in the deep part of the core. Taking $U_{\rm tw} = 10^3$ (or $0.58\,{\rm mm\,s^{-1}}$ if using $R_0 = 3480\,{\rm km}$ and $\eta = 2\,{\rm m^2\,s^{-1}}$ as the Earth's parameters) for instance, about 6 times faster than this simulation result, in which $U_{\rm tw} \simeq 180$, $\delta_{\rm jet} \simeq 1/40$ and $U_{\rm jet} \simeq 700$, and assuming that $H_{\rm jet}$ and $D_{\rm jet}$ are unchanged in all cases, one can obtain a jet of width $\delta_{\rm jet} R_0 = 15\,{\rm km}$ and of speed $U_{\rm jet}\eta/R_0 = 1.2\,{\rm cm\,s^{-1}}$ in the Earth's core. This speed is tens of times faster than usually conjectured. Of course this estimation relies on the assumption that the jet observed in this study is not controlled by viscosity at all, and that it is found in an asymptotic regime of low-E magnetoconvection. Detailed discussion of jets in the Earth's core is therefore beyond the scope of this study.

3.6. *Calculation varying other parameters*

A numerical simulation is carried out with the same parameters, but $\Lambda = 0.2$. The critical Rayleigh number becomes greater than 300 for this parameter set. Nevertheless, finite-amplitude convection occurs because a numerical solution for the previous run at $\Lambda = 1$ is used as the initial condition. As shown in figure 8, the convection flow after saturation is slightly suppressed compared to the case of $\Lambda = 1$. No strong and narrow jets occur during the simulation period. In figure 8,

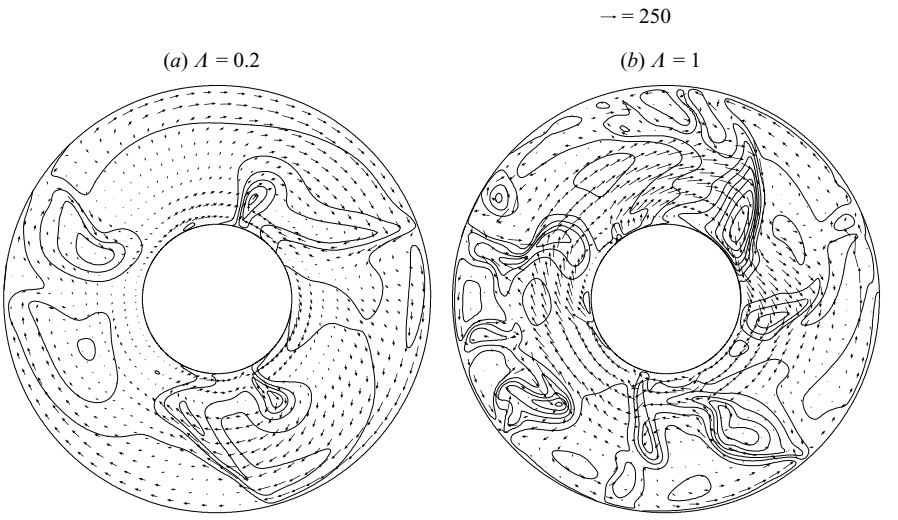

FIGURE 8. Axial magnetic fields (contours) and velocities (arrows) on the equatorial plane at (*a*) $\Lambda = 0.2$ and (*b*) $\Lambda = 1$, the latter being a snapshot at $t = 0.145$. The contour interval is 0.5; a unit arrow length (shown in the title) corresponds to $|\boldsymbol{u}| = 250$.

two notable upwelling plumes issue from the inner-core surface. The axial magnetic field is intensified at the west side of each plume. Downward ($u_s < 0$) plumes from the CMB are also found. Clockwise (anticyclonic) circulations superimposed on a westward zonal flow are evident with the magnetic field concentrated there. Although this is a similar characteristic to the previous simulation, an important difference is that stationary vortices beneath the CMB are absent because the westward zonal flow is developed in the entire the equatorial plane. Hence, the magnetic field concentrated in the anticyclone is advected monotonically, which means that no collision occurs between vortices and its steep gradient in the west side of the anticyclone. This is a possible explanation for the reduction of the downward jets.

In conclusion, an electric current sheet requires a steep gradient of an axial magnetic field that is caused by the collision of a magnetized anticyclonic vortex with an unmagnetized cyclone in the equatorial region. The Lorentz force normal to the current sheet is balanced by the Coriolis force that is produced by a narrow jet parallel or antiparallel to the electric current. Formation of a thinner jet depends on the relative velocity of the vortices.

4. Concluding remarks

The jet described in this paper is found to result from nonlinear interactions between a westward zonal flow and a hollow anticyclone in which an axial magnetic field is concentrated. Suppression of inertial and viscous forces in the presence of the prominent effect of Coriolis and Lorentz forces is important for jet formation. Zonal flows are also found in numerical models of self-exciting Earth-type dynamos and are regarded as a thermal wind that depends on the ratio of the rotation rate and the buoyancy flux, not on diffusivities or magnetic fields (Aurnou *et al.* 2003), giving grounds for expecting the existence of magnetic fronts in self-exciting (non-magnetoconvective) dynamos. In the Earth's core, the flow is inferred to be highly

turbulent with some degree of odd-mode symmetry. Although the turbulence in the Earth's core is also a central issue to be investigated, in this study arguments have benefited from a logical leap in considering magnetic fronts in the real Earth: the idea of a magnetic front presented herein assumes that a large-scale magnetized anticyclone with even-mode symmetry collides with a stationary cyclone. Future studies should elucidate whether the frontal structure is universal, even in the Earth's turbulent state. Those studies should also elucidate whether the physical process, as illustrated in figure 7, is part of the self-sustaining geodynamo.

The jet observed in this paper extends in the axial direction to around $|z| < 0.3$, as seen in figure 3, but not to the outer boundary of the fluid shell. Therefore, we cannot see a sharp variation of the magnetic field from outside the core. However, the situation might be different if the jet were thinner and more rapid, as expected under an Earth-like condition. It would also be interesting to investigate what type of magnetic field pattern and variation is observed at the Earth's surface when the jet structure emerges. The jet involves high-Reynolds-number flows. Therefore, its stability is also a concern. In our other simulation result, a jet-like flow triggered a breakdown of the even-mode symmetry of the convection pattern. This breakdown might be of particular importance in considering a temporal change of the geomagnetic field because an axial flow penetrating the equatorial plane, which belongs to an odd-mode symmetry, is thought to be related to excursions and polarity reversals (Li, Sato & Kageyama 2002).

A similar jet was shown in laboratory experiments on rotating non-magnetic thermal convection in a hemispherical shell driven by heterogeneous cooling from outside (Sumita & Olson 1999, 2002). In those experiments, a prograde flow was induced by local cooling at the CMB and a sharp front formed in the downstream side, thereby separating cold and hot regions in the fluid shell. A narrow jet flows from the outer to inner boundaries along the front. Its speed and width are estimated respectively as $\sim 1\,\mathrm{cm\,s^{-1}}$ and $\sim 2\,\mathrm{km}$ for the Earth. This jet is of thermal origin. Nevertheless, its speed and width are very similar to our results because both systems are fundamentally governed by an advection–diffusion equation with a strong zonal flow. When a magnetic field is imposed on this system, it is probable that a magnetized anticyclonic vortex is created in the eastern side of the front and the jet is modified by an induced magnetic field. Olson & Glatzmaier (1996) considered magnetoconvection, driven by heterogeneous heat flows on the CMB. That study found no frontal structures, probably because of the large Ekman number (2.1×10^{-4} in our definition).

Magnetohydrodynamic shear layers and jets are found in a spherical Couette flow, with the outer spherical surface fixed and the electrically conductive inner core rotating (Dormy *et al.* 1998; Hollerbach & Skinner 2001; Dormy, Jault & Soward 2002). When a strong magnetic field is imposed on this system, the angular velocity of the fluid tends to be constant along a line of magnetic force (Ferraro's law of isorotation). The inner and outer spherical boundaries rotate with different angular velocities. Therefore, a shear layer emerges between the region in which the field lines cross both the boundaries and the region in which the field lines cross either inner or outer boundaries. When an axial dipole field of internal origin is applied, for example, a super-rotating (prograde) thin jet flows in the shear layer; that flow is attributable to the Hartmann current circulating through the fluid spherical shell. In our case, a sheet-like electric current also plays an important role in jet formation. However, the super-rotating jet is peculiar to the case of an infinite Elsasser number, where the Coriolis force is absent. These two jets differ markedly in the way that the Lorentz force is balanced.

Another example to be compared is a wall jet in a rotating fluid (Stern, Chassignet & Whitehead 1997). This jet is injected mechanically from a point source on a vertical wall. It flows along the wall to some distance accompanying two-dimensional small-scale eddies, but it detaches abruptly from the wall, thereby producing a turbulent plume that is normal to the wall. Although the jet is produced artificially in this example, such an intrinsic property of a strong flow concentrated near a boundary wall might give some insight into our jet because it tends to originate from the CMB abruptly (see figure 8). It is noteworthy, however, that our jet is free from viscous effects and is entirely different from the non-magnetic wall jet that is controlled by viscosity.

The jet structure shown in figures 6 and 7 suggests behaviour corresponding to a simple advection–diffusion equation like a one-dimensional Burgers equation with small diffusivity. This interpretation might provide a simple and clear viewpoint, but it is a broad one. This study revealed a significant effect of induction caused by a vertical jet and the dominance of Coriolis and Lorentz forces over an inertial force, which represent unique characteristics of the jet. It is noteworthy that the relative importance of the inertial force to the Lorentz force is measurable using the ratio of kinetic to magnetic energy densities as shown by (3.6); this ratio is proportional to the (magnetic) Ekman number, provided that typical magnetic Reynolds and Elsasser numbers are constants. Hence, the jet formation is peculiar to magnetoconvection in a system of low Ekman number, probably 10^{-6} or lower, in which the magnetic energy is intrinsically much greater than the kinetic energy. With a larger Ekman number, we were unable to find a jet because of the growth of an inertial force, which would smooth out the rapid jet-like flow.

The jet is so thin that it is difficult to have adequate spatial resolution in computer simulations, which might be another reason why previous studies have not revealed this phenomenon. The spatial resolution in this calculation is perhaps a minimum requirement for simulating the jet (e.g. just a few Chebyshev collocation points exist in the Ekman layer beneath the CMB). This study provides a concrete illustration of fine structure in rotating magnetoconvection and suggests the importance of high-resolution calculations in modelling the geodynamo.

Computer simulations were performed at the Earth Simulator Center, Japan Agency for Marine-Earth Science and Technology. This study was partly supported by a JSPS Grant-in-Aid for Scientific Research.

REFERENCES

Aubert, J. 2005 Steady zonal flows in spherical shell dynamos. *J. Fluid Mech.* **542**, 53–67.

Aubert, J., Brito, D., Nataf, H.-C., Cardin, P. & Masson, J.-P. 2001 A systematic experimental study of rapidly rotating spherical convection in water and liquid gallium. *Phys. Earth Planet. Inter.* **128**, 51–74.

Aurnou, J., Andreadis, S., Zhu, L. & Olson, P. 2003 Experiments on convection in Earth's core tangent cylinder. *Earth Planet. Sci. Lett.* **212**, 119–134.

Cardin, P. & Olson, P. 1995 The influence of toroidal magnetic field on thermal convection in the core. *Earth Planet. Sci. Lett.* **132**, 167–181.

Chandrasekhar, S. 1961 *Hydrodynamic and hydromagnetic stability*. Oxford: Clarendon Press.

Dormy, E., Cardin, P. & Jault, D. 1998 MHD flow in a slightly differentially rotating spherical shell with conducting inner core in a dipolar magnetic field. *Earth Planet. Sci. Lett.* **160**, 15–30.

Dormy, E., Jault, D. & Soward, A. M. 2002 A super-rotating shear layer in magnetohydrodynamic spherical Couette flow. *J. Fluid Mech.* **452**, 263–291.

Fearn, D. R. 1979 Thermal and magnetic instabilities in a rapidly rotating sphere. *Geophys. Astrophys. Fluid Dyn.* **14**, 103–126.

Glatzmaier, G. A. & Roberts, P. H. 1995 A three-dimensional self-consistent computer simulation of a geomagnetic field reversal. *Nature* **377**, 637–640.

Hollerbach, R. & Skinner, S. 2001 Instabilities of magnetically induced shear layers and jets. *Proc. R. Soc. Lond.* A **457**, 785–802.

Hulot, G., Eymin, C., Langlais, B., Mandea, M. & Olsen, N. 2002 Small-scale structure of the geodynamo inferred from Oersted and Magsat satellite data. *Nature* **416**, 620–623.

Ishihara, N. & Kida, S. 2002 Dynamo mechanism in a rotating spherical shell: competition between magnetic field and convection vortices. *J. Fluid Mech.* **465**, 1–32.

Kageyama, A., Sato, T., Watanabe, K., Horiuchi, R., Hayashi, T., Todo, Y., Watanabe, T. H. & Takamaru, H. 1995 Computer simulation of a magnetohydrodynamic dynamo. II. *Phys. Plasmas* **2**, 1421–1431.

Kono, M. & Roberts, P. H. 2002 Recent geodynamo simulations and observations of the geomagnetic field. *Rev. Geophys.* **40**, 1013, doi:10.1029/2000RG000102.

Kuang, W. & Bloxham, J. 1997 An Earth-like numerical dynamo model. *Nature* **389**, 371–374.

Li, J., Sato, T. & Kageyama, A. 2002 Repeated and sudden reversals of the dipole field generated by a spherical dynamo action. *Science* **295**, 1887–1890.

Olson, P. & Glatzmaier, G. A. 1995 Magnetoconvection in a rotating spherical shell: structure of flow in the outer core. *Phys. Earth Planet. Inter.* **92**, 109–118.

Olson, P. & Glatzmaier, G. A. 1996 Magnetoconvection and thermal coupling of the earth's core and mantle. *Phil. Trans. R. Soc. Lond.* A **354**, 1413–1424.

Sakuraba, A. 2002 Linear magnetoconvection in rotating fluid spheres permeated by a uniform axial magnetic field. *Geophys. Astrophys. Fluid Dyn.* **96**, 291–318.

Sakuraba, A. & Kono, M. 1999 Effect of the inner core on the numerical solution of the magnetohydrodynamic dynamo. *Phys. Earth Planet. Inter.* **111**, 105–121.

Sakuraba, A. & Kono, M. 2000 Effect of a uniform magnetic field on nonlinear magnetoconvection in a rotating fluid spherical shell. *Geophys. Astrophys. Fluid Dyn.* **92**, 255–287.

Sarson, G. R., Jones, C. A., Zhang, K. & Schubert, G. 1997 Magnetoconvection dynamos and the magnetic fields of Io and Ganymede. *Science* **276**, 1106–1108.

Stellmach, S. & Hansen, U. 2004 Cartesian convection driven dynamos at low ekman number. *Phys. Rev.* E **70**, 056312.

Stern, M. E., Chassignet, E. P. & Whitehead, J. A. 1997 The wall jet in a rotating fluid. *J. Fluid Mech.* **335**, 1–28.

Sumita, I. & Olson, P. 1999 A laboratory model for convection in Earth's core driven by a thermally heterogeneous mantle. *Science* **286**, 1547–1549.

Sumita, I. & Olson, P. 2002 Rotating thermal convection experiments in a hemispherical shell with heterogeneous boundary heat flux: implications for the Earth's core. *J. Geophys. Res.* **107**, 2169, doi:10.1029/2001JB000548.

Sumita, I. & Olson, P. 2003 Experiments on highly supercritical thermal convection in a rapidly rotating hemispherical shell. *J. Fluid Mech.* **492**, 271–287.

Walker, M. R. & Barenghi, C. F. 1997 Magnetoconvection in a rapidly rotating sphere. *Geophys. Astrophys. Fluid Dyn.* **85**, 129–162.

Walker, M. R. & Barenghi, C. F. 1999 Nonlinear magnetoconvection and the geostrophic flow. *Phys. Earth Planet. Inter.* **111**, 35–46.

Zhang, K. 1995 Spherical shell rotating convection in the presence of a toroidal field. *Proc. R. Soc. Lond.* A **448**, 245–268.

Zhang, K. & Schubert, G. 2000 Magnetohydrodynamics in rapidly rotating spherical systems. *Annu. Rev. Fluid Mech.* **32**, 409–443.